ACS SENSORS

pubs.acs.org/acssensors Article

Sweat-Based Noninvasive Skin-Patchable Urea Biosensors with Photonic Interpenetrating Polymer Network Films Integrated into PDMS Chips

Saddam Hussain and Soo-young Park*

Cite This: https://dx.doi.org/10.1021/acssensors.0c01757 Read Online

ACCESS | Metrics & More | Article Recommendations | Supporting Information

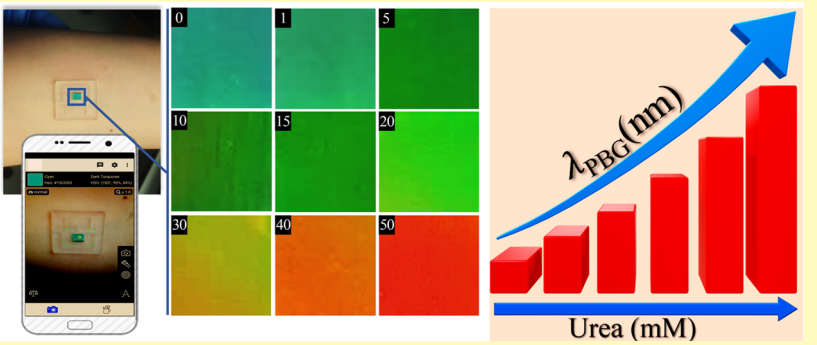

ABSTRACT: A wearable noninvasive biosensor for in situ urea detection and quantification was developed using a urease-immobilized photonic interpenetrating polymer network (IPN_{urease}) film. The photonic IPN film was intertwined with solid-state cholesteric liquid crystals (CLC_{solid}) and a poly(acrylic acid) (PAA) network on a flexible poly(ethylene terephthalate) substrate adhered to a poly(dimethylsiloxane) (PDMS) chip that was fabricated using an aluminum mold. The presence of urea in the chemical matrix of human sweat red-shifted the reflected color of the photonic IPN_{urease} film, and quantification was achieved by observing the wavelength at the photonic band gap (λ_{PBG}) with a limit of detection of 0.4 mM and a linear range of 0.9−50 mM. The color changes observed in the photonic IPN film were digitalized using the CIE 1931 *xy* coordinates on a cell phone image, thereby enabling fast, direct diagnosis via a downloadable app. This novel PDMS chip can be expanded for use with other biosensors.

KEYWORDS: *photonic crystal, interpenetrating polymer network, flexible, biosensor, urea, cholesteric liquid crystal*

Thin, flexible, biocompatible, and nonirritating sensing devices that can be worn directly on human skin are of keen interest in the healthcare industry, particularly for continuous monitoring applications[1−5] as the human skin provides an easy route for the diagnosis of diseases.[6] Ideally, skin-patchable devices should be stretchable up to 15% of the strain level to facilitate the full range of motion in humans.[7] Various fabrication methods, including jet printing, tattooing, and printing on cloths and papers, as well as lithography using microfluidics, have been employed for the manufacturing of wearable sensors.[8−13] Among these established technologies, lithography with microfluidics is of particular interest to researchers as it facilitates the precise fabrication of narrow channels and improves the reservoir capabilities of the device. In the study conducted by Rogers et al., soft epidermal poly(dimethylsiloxane) (PDMS) microfluidic devices were fabricated for sweat collection and analysis.[13] Here, the bottom PDMS layer was engraved and filled with the color-responsive reagent for colorimetric analysis before being connected to narrow channels that drained excess sweat away from the skin of the wearer.

Bodily fluids such as urine, saliva, tears, and sweat have long been used as representative analytes for the diagnosis of various diseases.[14] In particular, sweat is an excellent diagnostic aid as it is rich in electrolytes, biomolecules, and small organic molecules and can be utilized for noninvasive sample collection methods[15,16] of the analytes commonly found in sweat, namely, lactate, zinc, ammonium, alcohol, sodium, potassium, glucose, calcium, and uric acid,[17] and urea is seen as a key diagnostic agent as it is produced from the metabolism of nitrogen-based biomolecules in the human liver.[18] Although the primary mode of excretion is in the form of urine via the kidneys, urea is also secreted in bodily fluids such as sweat, blood, and saliva.[19] Since urea is an important biomarker for diagnosing kidney and liver

Received: August 23, 2020
Accepted: November 16, 2020

Scheme 1. Preparation Procedures of the Photonic IPN Film on the Flexible PET Substrate[a]

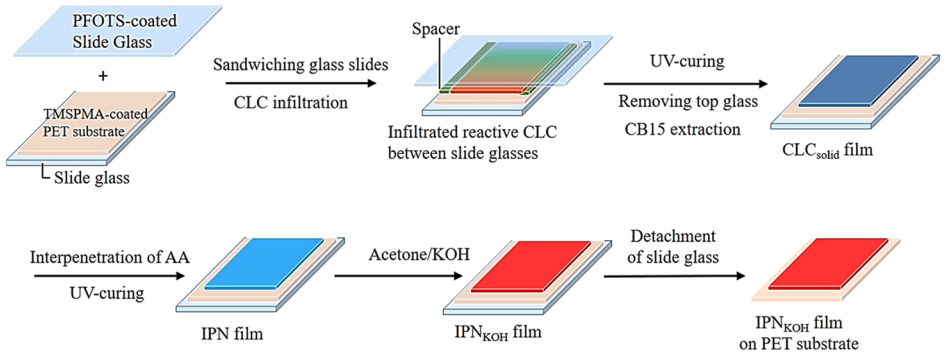

[a]Affixing the PFOTS-coated glass to the TMSPMA-Coated PET Film with a 20 μm Gap to Make a Glass Slide Shell, Infiltration of the Reactive CLC Mixture, UV Curing, Detachment of the PFTOS-Coated Glass, Extraction of the Chiral Dopant, Interpenetration of the AA Mixture, UV Curing, Acetone/KOH Treatment, and Detachment of the Photonic IPN_{KOH} Film on the PET Substrate from the Slide Glass.

issues,[20] elevated levels in sweat (a condition referred to as "uremia") are symptomatic of chronic kidney and renal diseases.

Wearable electrochemical array sensors integrated into flexible silicone[21] or laser-engraved thin film[22] were used for the continuous monitoring of the human healthcare system in prolonging indoor and outdoor physical activities. However, the electrochemical sweat sensors contain electrodes, wires, and other electronic components printed on flexible circuit boards and need power supplies and data communication hardware.[23] Several electrochemical and optical sensors have been developed for the detection of urea, most of which are either based on a bienzymatic (typically urease and glutamate dehydrogenase) system on rigid electrodes (electrochemical)[24] or contain a pH-responsive dye or urease immobilized on paper strips (optical).[25] Unfortunately, these devices are less than ideal. Electrochemical sensors are notoriously complex to operate because the electrodes must be connected to the small test site via conducting lines. On the other hand, optical biosensors lack the sensitivity required to detect small changes in the concentration of urea.[26,27] Recently, a photonic biosensor array system based on an interpenetrating polymer network (IPN) affixed to a glass substrate was developed.[28] The biosensor consisted of solid-state cholesteric liquid crystals (CLC_{solid}) intertwined with the weak anionic polyelectrolyte network of cross-linked poly(acrylic acid) (PAA) molecules. The CLC_{solid} and PAA networks are responsible for the reflected photonic color and volumetric changes that occur in response to external stimuli, respectively. Alterations in the helicoidal pitch and the reflected photonic color of CLC_{solid} are triggered by volumetric changes of the PAA network, which swells at high pH due to increased electrostatic repulsion between the ionized carboxylic groups and shrinks at low pH due to the presence of hydrogen-bonding interactions between the carboxylic groups. PAA is also quite reactive, forming covalent bonds between its carboxylic groups and enzymes via 1-ethyl-3-(3-dimethylaminopropyl)carbodiimide (EDC)-mediated coupling reaction. Urease-immobilized photonic IPN array films on glass substrates have shown excellent urea-detecting ability that was characterized by a reflected color change in response to urea in human serum. However, these urease-immobilized photonic IPN films can only function as wearable sensors when the photonic IPN structure is applied on a flexible substrate.[29]

Herein, we developed a urease-functionalized photonic IPN sensor on a flexible poly(ethylene terephthalate) (PET) substrate integrated into a PDMS chip for the detection of urea in human sweat. The PDMS chip was designed to be directly affixed to the human skin as a wearable biosensor that collected sweat from the skin via imprinted channels. The detection of urea was visualized through the photonic IPN sensor via color changes. This simple PDMS chip exhibited excellent adhesive properties to human skin and outstanding urea detection capabilities with faster response times; one key advantage offered by this chip was the need for only a small amount of the sweat sample for analytical purposes. Most notably, urea quantification was done without any sophisticated analytical instruments, and naked-eye detection was facilitated by digitally integrating the results using a cellular phone and a downloadable app.[30−35] This cost-effective, simple sensor is ideal for the easy, noninvasive screening of urea-related diseases using human sweat, and it can be expanded for other diagnostic purposes by changing the immobilized receptors/enzymes in the photonic IPN sensors.

EXPERIMENTAL SECTION

Materials. Trichloro(1*H*,1*H*,2*H*,2*H*-perfluoroctyl)silane (PFOTS, 97%), 3-(trimethoxysilyl)propyl methacrylate (TMSPMA, 98%), *N*-hydroxysuccinimide (NHS), (3-dimethylaminopropyl)-*N*′-ethylcarbodiimide hydrochloride (EDC·HCl), D-(+)-glucose, urea, urease, acrylic acid (AA), tripropylene glycol diacrylate (TPGDA), zinc nitrate hexahydrate ($Zn(NO_3)_2{\cdot}6H_2O$), magnesium nitrate hexahydrate ($Mg(NO_3)_2{\cdot}6H_2O$), and sodium lactate were purchased from Sigma-Aldrich and used without further purification except for AA and TPGDA, which were used after removing the inhibitor by passing through a column of activated alumina. Reactive mesogen (RMM727, Merck, U.K.), (*S*)-4-cyano-4′-(2-methylbutyl)biphenyl (CB15, Synthon, Germany), photoinitiator Irgacure 500 (Ciba, Switzerland), double-sided adhesive spacer (Spacer (20 μm), Nitto), bare glass slides (Paul Marienfeld GmbH, Germany), buffer solutions (pH 2−12, Samchun, South Korea), acetone (Duksan, South Korea), iron(II) chloride tetrahydrate ($FeCl_2{\cdot}4H_2O$, Samchun, South Korea), and sodium chloride (NaCl, Duksan, South Korea) were used without further purification. Sylgard 184 silicone elastomer base kit and Sylgard 184 silicone elastomer curing agent were purchased from Dow. Deionized (DI) water was purified using a μPure reverse-osmosis system (Romax, South Korea). RMM727 was completely mixed with CB15 (29.5 wt %) by magnetic stirring for 4 h at 50 °C to obtain a transparent mixture that was then cooled to 20 °C for future experiments. A mixture consisting of the AA monomer (98.5 wt %), TPGDA (0.5 wt %), and Irgacure 500 (1 wt %) was used for the PAA network in the IPN film after magnetic stirring at 400 rpm and 20 °C for 2 h.

Preparation of the Photonic IPN on the PET Substrate. The photonic IPN film on the flexible PET substrate was prepared, as shown

https://dx.doi.org/10.1021/acssensors.0c01757
ACS Sens. XXXX, XXX, XXX−XXX

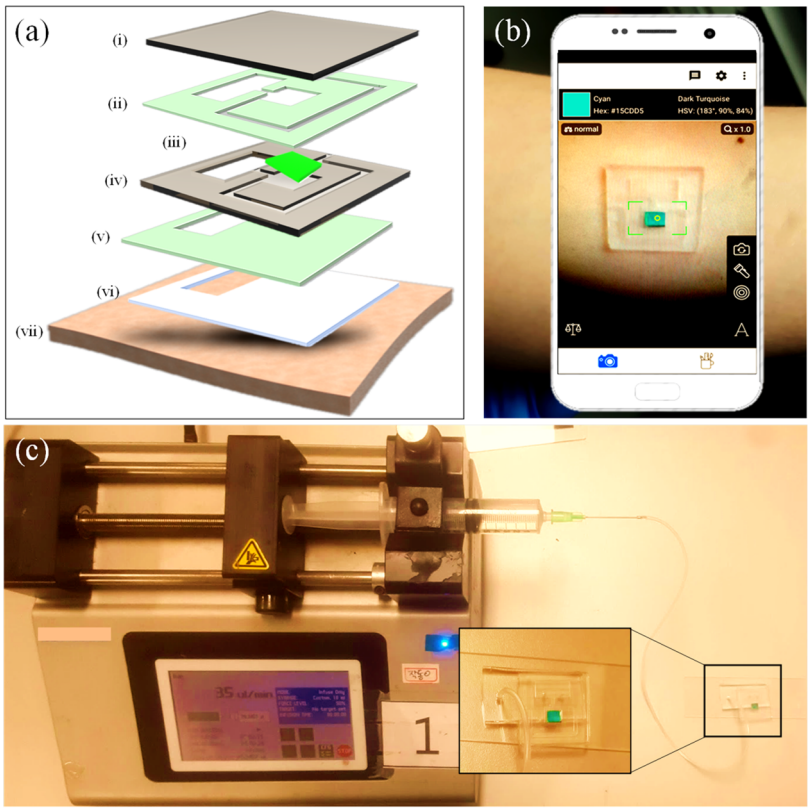

Figure 1. (a) Schematic of the multilayered PDMS chip consisting of the (i) PDMS top cover, (ii) double-sided tape, (iii) photonic IPN_{urease} film, (iv) patterned PDMS layer, (v) medical-grade double-sided adhesive tape, and (vi) temporary protective paper on (vii) human epidermis. (b) Photographs of the PDMS chip on a volunteer's forearm while taking a picture using a cellular phone for the in situ analysis of the reflected color of the photonic IPN film. (c) Experimental setup for the detection of urea. The inset shows the enlarged PDMS chip connected to the syringe pump.

in Scheme 1. Briefly, the PET film was rinsed with water and ethanol. The clean PET film was fixed on the glass slide using double-sided adhesive tape to make the PET film lie flat on the glass for future treatment. The TMSPMA-coated PET film surface was prepared via the following steps: (i) Oxygen plasma treatment for 5 min (CUTE, Femto Science, South Korea) was conducted. (ii) Spin-coating with TMSPMA was performed, followed by calcination at 110 °C for 5 min using an oven (DWO-G13SS, Daewoo, South Korea). The PFOTS-coated upper glass slide was prepared by rinsing the glass slide with ethanol and subsequent O_2 plasma treatment for 5 min before transferring the treated glass slide to a sealed container containing 7 μL of PFOTS reagent, followed by heating in an oven (G1708A01090120, Daewoo, South Korea) for 2 h at 70 °C. The PFOTS-coated glass was affixed to the TMSPMA-coated PET film with a 20 μm gap by a 20 μm double-sided adhesive plastic spacer. The gap between the PFOTS-coated glass and the TMSPMA-coated PET film was filled with a reactive CLC mixture containing RMM727 (70.6 wt %) and CB15 (29.4 wt %). After complete infiltration of the reactive CLC mixture via capillary force through the gap, the reactive CLC mixture was photopolymerized under UV light at 365 nm using an Innocure 100N UV-curing machine (Lichtzen, South Korea). The PFOTS-coated glass was then removed, and the chiral dopant was extracted by washing the CLC film with acetone to generate the CLC_{solid} film on the PET substrate. The AA mixture was poured onto the CLC_{solid} film on the PET substrate to encourage impregnation and was subsequently subjected to UV polymerization for 15 min at an intensity of 22 mW/cm^2. The prepared photonic IPN film on the PET substrate was immersed in a buffer solution (pH 7) to remove any excess hydrogel from the surface. This was done because the PAA network swells in the pH 7 buffer solution, thereby facilitating the easy removal of excess PAA from the film. An acetone wash was done to increase the sensitivity of the film and the intensity of the reflected color change.[36] The prepared photonic IPN film on the PET substrate was further treated with 1 M KOH aqueous solution (IPN_{KOH}) for 30 min to facilitate the complete expansion of the PAA network.[37] The flexible photonic IPN_{KOH} film on the PET substrate was then detached from the glass slide and used as a sensor for sweat analysis.

Preparation of the Urease-Immobilized Photonic IPN Films. Immobilization of urease on the photonic IPN film was conducted using an EDC/NHS coupling method.[28] Briefly, aqueous solutions of EDC·HCl (0.2 M) and NHS (0.2 M) were mixed in a 1:2 (v/v) ratio with magnetic stirring at 500 rpm for 40 min at 20 °C. The resulting EDC/NHS mixture (15 μL) was added dropwise to the 5 × 5 mm^2 photonic IPN film and left to stand for 1 h at 25 °C, after which the photonic IPN film was wiped off with a tissue. Subsequently, an aqueous solution of urease (60 μM, 15 μL) was added dropwise to the surface of the photonic IPN film and left to stand for 2 h to facilitate covalent immobilization. The resulting photonic IPN_{urease} film was washed with DI water to remove any nonbonded urease and EDC/NHS components. All aqueous urea solutions were prepared in a buffer solution (pH 6) to mimic the pH of sweat during the urea detection tests.[38]

An aqueous urea solution (15 μL) was used to test the 5 × 5 mm^2 photonic IPN_{urease} film. The reflected color was observed 1 h after the urea solution was added dropwise to the photonic IPN_{urease} film, and the associated retention time was previously discussed in the Results and Discussion section. The limit of detection (LOD) for the photonic IPN_{urease} film was calculated using the following equation[39−41]

$$\mathrm{LOD} = 3.3 \times \left(\frac{\mathrm{SD}}{s}\right)$$

where SD is the standard deviation obtained from triplicate experiments that were tested with the blank (0 mM) urea solution as the control and s is the corresponding slope of the graph in Figure S7 (see the Results and Discussion section).

https://dx.doi.org/10.1021/acssensors.0c01757
ACS Sens. XXXX, XXX, XXX−XXX

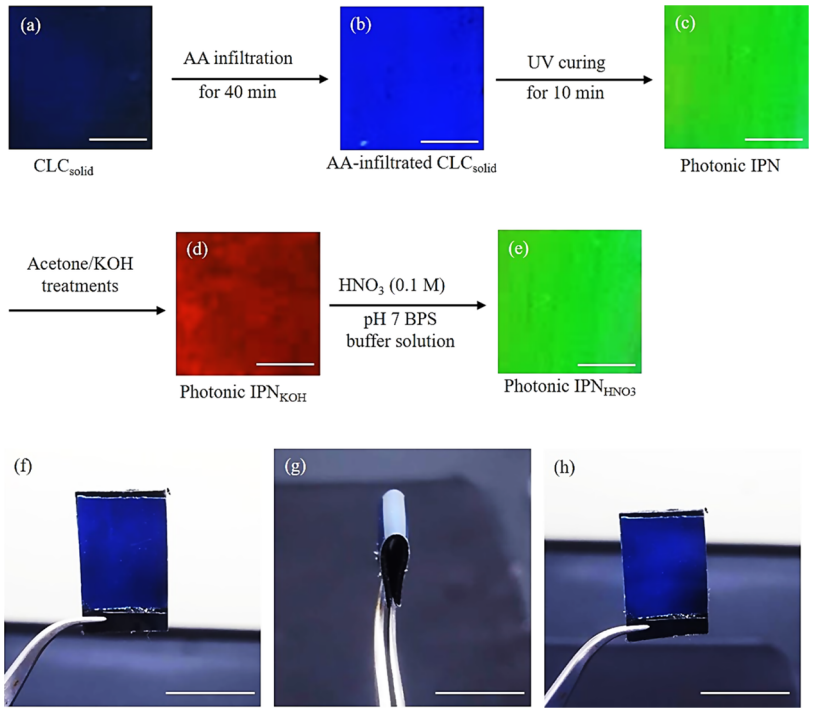

Figure 2. Photographs of the (a) CLC$_{solid}$, (b) AA-infiltrated CLC$_{solid}$, (c) photonic IPN, (d) acetone/KOH-treated photonic IPN (IPN$_{KOH}$), and (e) HNO$_3$/pH 7 buffer-treated photonic IPN (IPN$_{HNO3}$) films on a PET substrate. Photographs of the deformation tests conducted on the flexible photonic IPN film on the PET substrate in the (f) flat, (g) bent, and (h) restored states. The scale bars in (a–e) and (f–h) are 2 and 10 mm, respectively.

PDMS Chip for the Production of a Patchable Epidermal Sensor. A custom-designed aluminum mold was used for the production of the wearable PDMS chip. The computer-aided design (CAD) for the aluminum mold (Figure S1a) was done using AutoCAD (Autodesk, 2019). The aluminum mold (Figure S1b) was fabricated by mechanically milling an aluminum sheet in the dimensions of 30 (W) × 30 (L) × 3 (H) mm^3. The mold consisted of a sweat-collecting chamber (10 (W) × 5 (L) × 1 (H) mm^3) connected to a reservoir (5 (W) × 5 (L) × 0.5 (H) mm^3) through a narrow channel (2 (L) × 1 (W) × 0.5 (H) mm^3). The total volume of the reservoir was 12.5 mm^3. The reservoir was connected to the outside through a drainage channel for the excess sweat. The PDMS precursor was prepared by mixing the silicone elastomer base kit and the curing agent of Sylgard 184 at a ratio of 10:1 (w/w). The PDMS precursor was poured into the aluminum mold, which was then covered with the easily detachable PFOTS-coated glass and baked at 60 °C for 2 h. A uniform 1 mm thick PDMS chip with clear microchannels was peeled from the mold, and the photonic IPN$_{urease}$ film was affixed in the reservoir of the patterned PDMS chip. The patterned PDMS chip with the attached photonic IPN$_{urease}$ film inside the reservoir was covered with a flat PDMS layer using double-sided Tyco adhesive (3M), as shown in Figure S1c. Figure 1a illustrates the schematic for the preparation of the multilayered PDMS chip: (i) the top transparent and protective PDMS layers were attached to (iv) the patterned PDMS layer through (ii) double-sided adhesive tape to prevent the evaporation of sweat. The flexible photonic IPN$_{urease}$ film on (iii) the PET substrate was embedded in (iv) the reservoir of the patterned PDMS layer. The patterned PDMS layer contained the sweat-collecting chamber connected to the reservoir via a narrow drainage channel that drained sweat away from the sweat-collecting chamber to the reservoir. When the excess sweat overflowed from the reservoir, it could be drained outside via the channel's jet-outlet opening. (v) The double-sided medical-grade tape facilitated the adhesion of the PDMS chip directly to the skin, and (vi) its protective paper was peeled off when used. Figure 1b shows the photograph of the PDMS chip on a volunteer's forearm while taking a picture using a cellular phone to document the reflected color changes of the photonic IPN film. The aqueous urea solution (C_{urea} = 40 mM) was injected into the PDMS chip using a Legato 100 syringe pump (KD Scientific) directly connected to the sweat-collecting chamber via a narrow channel in the PDMS sheet, as shown in Figure 1c. Movie S1 shows the aqueous sweat traversing the PDMS chip from the collecting chamber to the reservoir via the drainage channel.

Measurements. The fractured cross-sectional surface of the photonic IPN layer was studied using field-emission scanning electron microscopy (FE-SEM, SU8220, Hitachi, Japan) after platinum coating for 100 s. The cross-sectional surface was obtained by cutting the film with a blade. Attenuated total reflection–Fourier transform infrared (ATR–FTIR) spectra were recorded in the range of 500–4000 cm^{-1} at an average of 64 scans using an FTIR spectrometer (FT/IR-4100, Jasco, Japan). The UV–vis absorbance spectra were recorded using a DH-2000-BAL lamp (Ocean Optics) in the range of 300–900 nm by placing the photonic IPN film perpendicular to the incident light beam. Photographs were obtained under humid conditions, i.e., fully immersed in water or sweat, using a cellular phone camera (Galaxy S6, Samsung, South Korea), as shown in Figure 1b. The reflected color was digitalized via the RGB and CIE xy coordinates of the photograph taken from the cellular phone using the Color Grab app (Loomatix, Israel). The xy coordinates of the image were plotted on the xy chromaticity diagram per the CIE 1931 system.[42] The dominant wavelength ($\lambda_{dominant}$) was determined by plotting a line between the chromaticity coordinates of the reference white point (R = 255, G = 255, B = 255, x = 0.3127, y = 0.3290) and the observed reflected color on the diagram and then extrapolating at the apex of the horseshoe-shaped curve.[43]

In Situ Human Sweat Test. In situ collection of sweat from human skin was conducted during indoor physical exercise using the PDMS sweat-collecting device with a storage capacity of 1 mL. The PDMS sweat-collecting device was almost identical to the PDMS chip, except for its larger storage capacity. The tests were conducted by sequentially cleansing the chest of the healthy human volunteer with water and ethanol to prevent contamination. Subsequently, the prepared device was attached to the cleaned section of the chest using a double-sided medical-grade adhesive, and the human sweat samples were collected during the indoor exercise.

https://dx.doi.org/10.1021/acssensors.0c01757
ACS Sens. XXXX, XXX, XXX–XXX

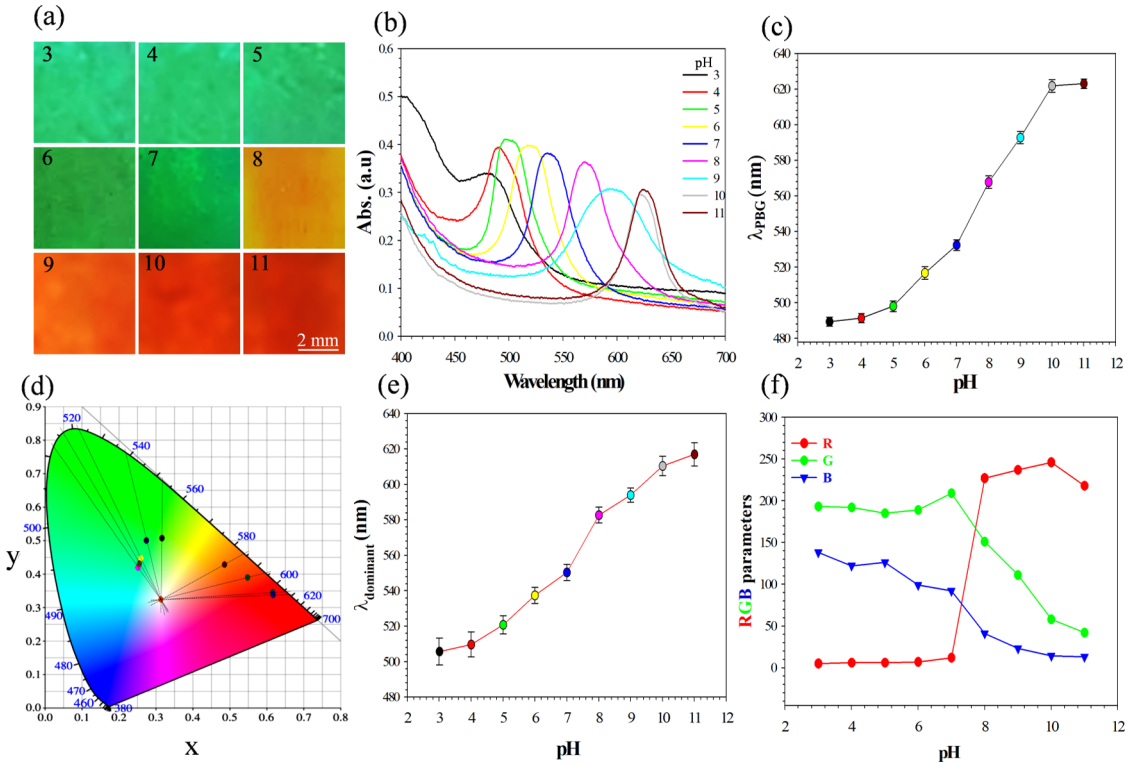

Figure 3. (a) Photographs and (b) the UV−vis spectra of the photonic IPN films at different pH levels; numbers in (a) represent pH. (c) λ_{PBG} values calculated using data from (b) as a function of pH. (d) *xy* chromaticity diagram obtained for the images in (a). (e) $\lambda_{dominant}$ values calculated using data from (d) plotted against pH. (f) RGB values calculated using data from (a) as a function of pH. The error bars in (c) and (e) represent the standard deviation of experiments conducted in triplicate.

In the in situ tests, the developed PDMS chip was directly attached to the forearm of a healthy volunteer (male, age 30) who had no medical history of uremia, chronic illnesses, or heart disease. Next, the volunteer was instructed to start physical activity. After doing a running exercise for 1 h, the change of the reflected color of the photonic IPN_{urease} film in the PDMS chip was evaluated. The concentration of urea (C_{urea}) in the donated sweat was measured via a Model 600E high-performance liquid chromatography system (HPLC) equipped with an RI Model 410 detector (Waters Co.); the standard curves of the aqueous urea solutions were observed (Figure S2). The donated sweat was diluted fourfold with DI water for HPLC analysis. The measured C_{urea} from the donated human sweat was 20 mM. The artificial human sweat sample was also prepared by mixing the ten major components in human sweat in a BPS solution (pH 6) with or without 50 mM urea added. The amounts of each component are listed in Table S1.

RESULTS AND DISCUSSION

Preparation of Photonic IPN Films on PET Substrates.

Figure 2 contains photographs of each step during the preparation of the photonic IPN films on PET substrates. The initial blue color of the CLC_{solid} on the PET substrate (Figure 2a) changed to bright blue after impregnation using the AA mixture (Figure 2b) due to the increased helical pitch of the CLC_{solid}. The AA-impregnated CLC_{solid} on the PET substrate was then UV-cured to make the photonic IPN film. When the photonic IPN film on the PET substrate was placed in a buffer solution at pH 7, a green color was noted (Figure 2c) due to the swelling of the PAA network intertwined in the CLC_{solid}. When treated with acetone and 1 M KOH solution for 30 min, the photonic IPN film became more sensitive[44] as the acetone/KOH-treated photonic IPN film showed a red color (Figure 2d) due to COO^-K^+ complex formation, which blocked hydrogen-bonding interactions between the carboxylic moieties and triggered swelling of the photonic IPN network. The swollen acetone/KOH-treated photonic IPN film returned to its original state after being subjected to 0.1 M HNO_3 and buffer solution (pH 7) treatments (Figure 2e). The photonic IPN film prepared on the PET substrate was flexible and remained stable after deformation tests were conducted, as shown in Figure 2f−h.

The confirmation of the layered photonic structure developed was obtained via SEM analysis. Figure S3a,b shows the SEM images of the cross-sectional surfaces of the CLC_{solid} and photonic IPN films, respectively. Here, well-developed, layered photonic structures were observed from the CLC_{solid} (Figure S3a) and the photonic IPN (Figure S3b) films. SEM analysis revealed that the photonic structure of CLC remained stable after UV curing/chiral dopant extraction, and an intertwining hydrogel polymer network was noted in the CLC_{solid}. *P* is that helical pitch that can be measured from the vertical distance between two layers in the SEM image. The average helical pitch (*P*) values were determined using ImageJ software by conducting three measurements at random positions. The average *P* values are 262 ± 2 and 284.4 ± 1.5 nm for the CLC_{solid} and photonic IPN films, respectively. The increased *P* value for the photonic IPN film indicated that successful infiltration of the PAA network had occurred without disturbing the layered photonic structure of CLC_{solid}.

The structural development of the photonic urease-immobilized IPN (IPN_{urease}, will be discussed later) film during sample preparation was studied in detail using FTIR spectroscopy. Figure S3c(i),(ii) shows the FTIR spectra of the CLC_{solid} films before and after the extraction of the chiral dopant, CB15, respectively. The −CN stretching peak of CB15 appeared at 2225 cm^{-1} before dopant extraction (Figure S3c(i)), whereas

https://dx.doi.org/10.1021/acssensors.0c01757
ACS Sens. XXXX, XXX, XXX−XXX

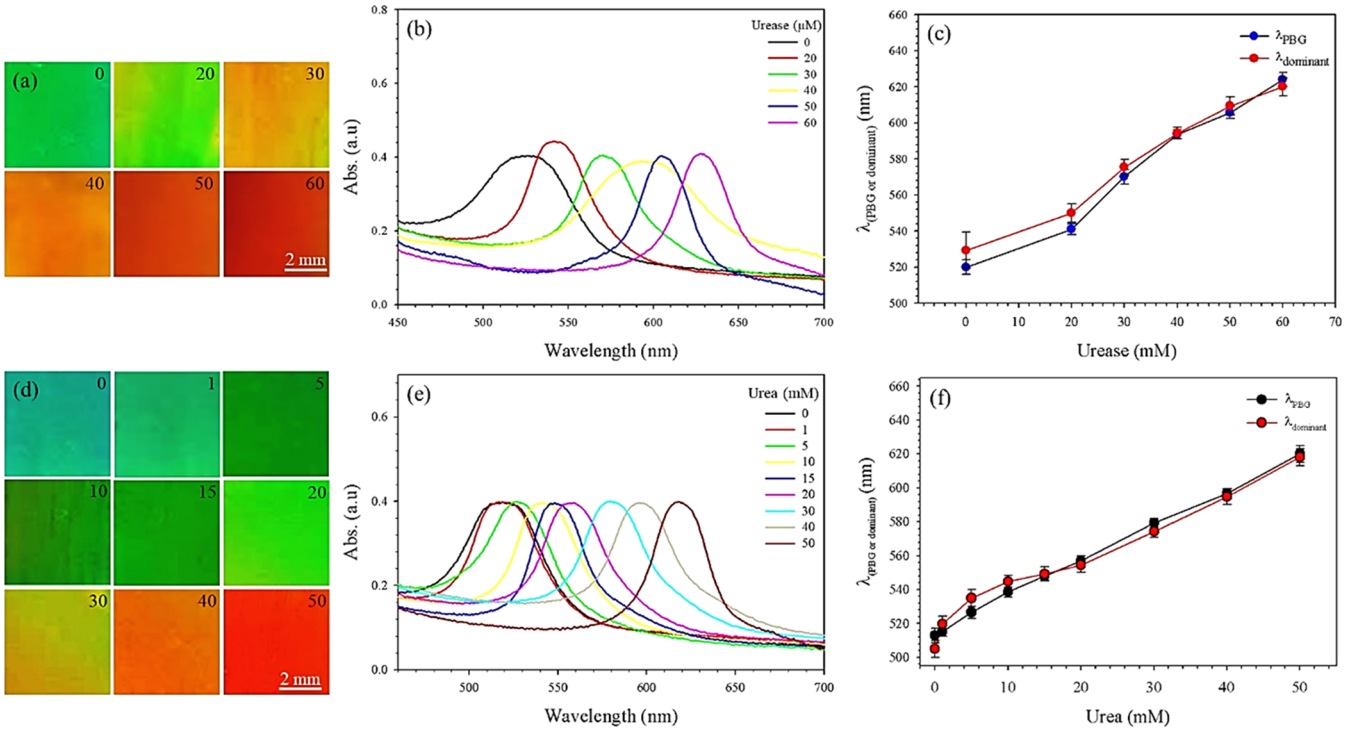

Figure 4. (a) Photographs and (b) UV−vis spectra of the photonic IPN_{urease} films prepared at various C_{urease} values. (c) $\lambda_{dominant}$ values of the cellular phone images (Figure S5a) and λ_{PBG} obtained from the UV−vis spectra of (b) as a function of C_{urease}. The photographs and UV−vis spectra were obtained 1 h after adding 50 mM aqueous urea (15 μL) to the photonic IPN_{urease} film dropwise. (d) Photographs and (e) UV−vis spectra of the photonic IPN_{urease} films 1 h after adding aqueous urea solutions (15 μL) containing different C_{urea} to the photonic IPN_{urease} film dropwise. (f) $\lambda_{dominant}$ values derived from the *xy* chromaticity diagram (Figure S5b) of the cellular phone images and λ_{PBG} obtained from the UV−vis spectra of (e) as a function of C_{urea}. The numbers in (a) and (d) represent C_{urease} and C_{urea}, respectively. The error bars in (c) and (f) represent the standard deviation of triplicate experimental results.

this peak disappeared after the extraction process (Figure S3c(i)), indicating that CB15 was completely removed by the acetone wash. Figure S3c(iii) shows the FTIR spectrum of the photonic IPN film. The peaks from PAA, namely, the stretching band of $-CH_2$ as well as the symmetric stretching bands of the C−O and C═O bonds, appeared at 1402, 1165, and 1725 cm^{-1}, respectively.[45] These peaks demonstrated the presence of the PAA networks. This result strongly suggests that the photonic IPN structure was formed. Amide-II N−H deformation and amide-I C═O stretching bands[46] were also observed in the photonic IPN_{urease} film (Figure S3c(iv)), indicating that urease had been successfully immobilized.

pH Responsiveness of the Photonic IPN Films. The pH responsiveness of the photonic IPN films was tested using phosphate-buffered saline (PBS) buffer solutions. Figure 3a shows the photographs of the photonic IPN films 40 min after buffer solutions (15 μL) at various pH levels were added to the film dropwise. The reflected color of the photonic IPN film red-shifted as the pH increased. Figure 3b shows the UV−vis spectra of the photonic IPN films at different pH levels. The peak position represents the wavelength at the photonic band gap (λ_{PBG}). Figure 3c exhibits the measured λ_{PBG} as a function of pH. The λ_{PBG} of the photonic IPN film continuously increased as the pH increased, indicating that the photonic IPN film was sensitive to pH changes and that its response could be read with the naked eye. These color changes observed in the IPN films were represented in the CIE 1931 *xy* chromaticity diagram shown in Figure 3d. Figure 3e shows the dominant wavelength ($\lambda_{dominant}$) values obtained from the CIE 1931 *xy* chromaticity diagram from Figure 3d as a function of pH. The relationship between the $\lambda_{dominant}$ and λ_{PBG} values was elucidated, and the associated correlation plot was obtained. Figure S4 shows the plot of the $\lambda_{dominant}$ as a function of λ_{PBG} for all data in this work. The linear regression equation was $y = 0.9432x + 31.8$ with r^2 of 0.99. The slope of the plot was close to 1, indicating that the measured $\lambda_{dominant}$ from a cellular phone image represented the λ_{PBG} obtained from UV−vis spectroscopy. Thus, the extent of the color change could be easily digitalized using the image taken from the cellular phone. The reflected color of the photonic IPN film could also be digitalized using the RGB values shown in Figure 3f. The "R" value increased as the pH increased, whereas the "G" and "B" components declined as the pH increased. No correlation was observed between the RGB values and λ_{PBG}. Thus, using the $\lambda_{dominant}$ for the relevant calculations was more convenient for cellular phone-based sensing applications than using the associated RGB values.

Urea Biosensors of the Photonic IPN_{urease} Film. Before the photonic IPN_{urease} film was tested with human sweat, the optimization of the amount of the immobilized urease was conducted. Figure 4a,b shows the photographs and the UV−vis spectra of the photonic IPN_{urease} films prepared at various urease concentrations (C_{urease}) 1 h after adding 50 mM aqueous urea (15 μL) to the photonic IPN_{urease} film dropwise. Figure 4c shows the $\lambda_{dominant}$ values obtained from the cellular phone images (Figure S5a) and the λ_{PBG} from the UV−vis spectra (Figure 4b) as a function of C_{urease}. Similar to the results seen in Figure 3, the $\lambda_{dominant}$ and λ_{PBG} values were very close to each other, indicating that the $\lambda_{dominant}$ obtained from the cellular phone image could be used to determine the λ_{PBG}. The λ_{PBG} (and $\lambda_{dominant}$) continuously increased from 520 to 620 nm as the C_{urease}

https://dx.doi.org/10.1021/acssensors.0c01757
ACS Sens. XXXX, XXX, XXX−XXX

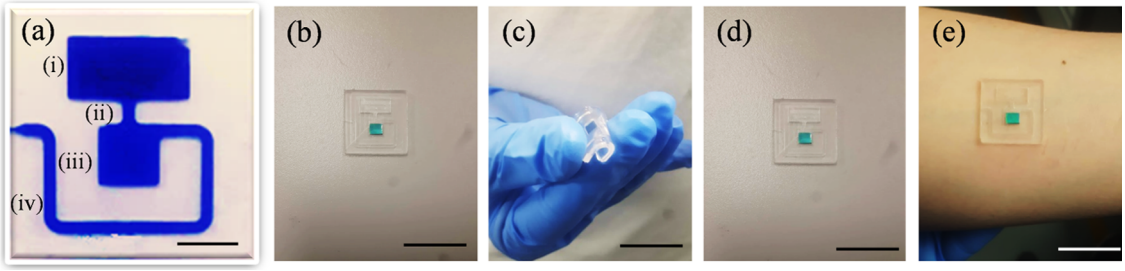

Figure 5. Photographs of the (a) top view of the PDMS chip filled with the blue-dyed aqueous solution in which the (i) sweat-collecting chamber, (ii) connecting channel, (iii) reservoir, and (iv) outlet channel can be seen. The PDMS chip (b) before and (c) after bending, (d) releasing the deformation, and (e) patching on the human epidermis as a wearable imaging device without any aqueous analyte. The scale bars in (a) and (b−e) are 5 μm and 20 mm, respectively.

increased from 0 to 60 μM. Since the urea concentration (C_{urea}) in human sweat is 22.4 mM under normal physiological conditions, a concentration of 50 mM is indicative of uremia.[19] The initial green color of the photonic IPN_{urease} film red-shifted as the C_{urease} increased, indicating that more ammonia was produced (i.e., the pH was increased) when more urease enzymes were immobilized. The green reflected color of the photonic IPN_{urease} film became red when C_{urease} was 60 μM. Thus, the photonic IPN film was subsequently immobilized with 60 μM aqueous urease for further studies. The speed of the color change of the photonic IPN_{urease} film was studied in relation to the time needed to achieve saturation of the reflected color after adding aqueous urea (50 mM, 15 μL) to the photonic IPN_{urease} film dropwise. Figure S6a,b shows the photographs of the photonic IPN_{urease} films and their associated UV−vis spectra at various retention times ($t_{retention}$). The corresponding λ_{PBG} values (Figure S6c) were measured using the data obtained from Figure S6b. The λ_{PBG} values continuously increased until the $t_{retention}$ was 60 min, after which saturation was noted at 620 nm. Therefore, all of the experiments were conducted at a $t_{retention}$ value of 60 min unless otherwise specified. The $t_{retention}$ of the current IPN_{urease} film is higher than that of the reported sensors. For example, colorimetric detection of urea in sweat was carried out with a urease-immobilized pH paper strip that was embedded in the skin-patchable PDMS microfluidic chip.[47] The urea analysis in sweat was based on the RBG values obtained from image processing, and the saturation time was optimized to 15 min. An electrochemiluminescence (ECL) flexible sensor was also developed by immobilizing highly luminescent nanospheres on Au nanotube networks that were integrated in the PDMS membrane.[48] The response time for the ECL flexible sensor was 6 min with a linear range from 45.0 μM to 19.5 mM. A flexible electrochemical sensor based on surface-imprinted nanotubes has also been reported.[49] The urea-templated molecular imprinted layer on the surface of the electrode increased the selectivity of the sensor. The value of current was linearly changed in the range of 0.1−100 mM urea concentration and the optimized response time was 15 min. However, these reported electrochemical sensors lack microfluidics channels, sweat-collecting chamber, and specific designs for sweat volume. The PDMS chip developed in this work for urea sensing in sweat has good microfluidic design and a photonic IPN film.

The response of the photonic IPN_{urease} film to urea was studied using aqueous solutions containing various urea concentrations (C_{urea}). Figure 4d and e shows the photographs and the UV−vis spectra of the photonic IPN_{urease} films 1 h after adding the aqueous urea solutions (15 μL) with different C_{urea}'s to the photonic IPN_{urease} film dropwise. Figure 4fc shows the $\lambda_{dominant}$ values (obtained from the cellular phone images, as seen in Figure S5b) and the λ_{PBG} values (obtained from the UV−vis spectra of Figure 4e) as a function of C_{urea}. Again, the $\lambda_{dominant}$ and λ_{PBG} values were similar. The λ_{PBG} linearly increased from 510 to 620 nm as the C_{urea} increased from 0 to 50 mM. The linear range/LOD values obtained from Figure S7 were 0.9−50/0.4 and 0.7−50/0.32 mM for λ_{PBG} and $\lambda_{dominant}$, respectively; this graph (Figure S7) was used as the standard curve for determining the urea concentration. Since these values were almost identical to each other, we concluded that either λ_{PBG} or $\lambda_{dominant}$ could be used to determine the urea content of human sweat. However, the $\lambda_{dominant}$ value was more convenient to obtain and was immediately available from the cellular phone image data.

Performance of the PDMS Chip. The accumulated volume of sweat in the PDMS chip was 81.75 μL. Generally, the sweating rate from the human epidermis is known to be 0.60 μL/min/gland, which includes approximately five glands in a 3 mm^2 area.[50] The 50 mm^2 collection chamber used in our study covered 83 sweat glands and facilitated the collection of 0.6 × 83 μL/min of sweat in 2.18 min. The PDMS chip was tested by injecting the methylene blue (dye) aqueous solution at a flow rate of 37 μL/min and was completely filled within 2.2−2.3 min, as shown in Figure 5a. Several design features were incorporated into the PDMS chip, namely, flexibility, transparency, and biocompatibility. In addition to its in situ urea detection capabilities, the chip was designed to collect and analyze sweat on human skin as its soft and flexible mechanics allowed for comfortable, nonirritating bonding to the human epidermis. To ensure that these parameters were met, we applied several deformation tests to the PDMS chip to determine its mechanical stability and flexibility. The initial PDMS chip (Figure 5b) was repeatedly contorted (Figure 5c) before being allowed to return to its original shape (Figure 5d). The PDMS chip was designed as a wearable device patch to facilitate easy, secure adherence to the human epidermis (Figure 5e). The patched PDMS chip biosensor conformed exceptionally well to the human epidermis and exhibited little to no signs of distress after being subjected to the deformation tests as it returned to the original shape without any loss in adherence. The reflected color of the photonic IPN_{urease} flexible film in the PDMS chip was unaffected by the applied deformations (for details, see Text S1 and Figure S8, Supporting Information).

The reusability and stability of the PDMS chip were measured via testing with aqueous urea at a C_{urea} value of 50 mM 0, 10, and 20 days after fabrication. The reusability of the PDMS chip was tested by passing 2 mL of PBS solution (pH 7) using a syringe

https://dx.doi.org/10.1021/acssensors.0c01757
ACS Sens. XXXX, XXX, XXX−XXX

pump at a flow rate of 20 μL/min for 100 min. The tested PDMS chips were kept at 8 °C in a sealed container for longer stability tests. Figure S9 shows the $\lambda_{dominant}$ and λ_{PBG} values of the PDMS chip with the urea and subsequent PBS buffer (pH 7) aqueous solution treatments (with real photographs in the inset) 0, 10, and 20 days after fabrication. The $\lambda_{dominant}$ (and λ_{PBG}) values were 615 (620), 613 (615), 516 (518), and 520 (519) nm after the urea/PBS buffer aqueous solution treatments for the 0-, 10-, and 20-day samples, respectively. The red reflected color observed after an aqueous urea treatment returned to the initial green color after being subjected to the above-mentioned PBS solution (2 mL). This complete recovery occurred even 20 days after fabrication, indicating that the prepared PDMS chips were stable for at least 20 days.

Cellular Phone Measurements. Since cellular phone images were used for the quantitative analysis of urea in our study, the effects exerted by the prevailing conditions during the "photoshoot" were investigated. The cellular phone camera was kept vertically (90°) against human skin as much as possible, although a little variation was unavoidable. First, the effect of the shooting distance was examined, as shown in Figure S10a. The $\lambda_{dominant}$ values were 495, 493, 491, 492, 489, and 490 nm at the sample-to-camera distances of 5, 10, 15, 20, 25, and 30 cm, respectively, indicating that the shooting distance did not significantly affect the cellular phone sensing, whereas camera focus was of utmost importance. Next, the influence of light was studied under various light conditions such as inside the laboratory, in bright sunlight, in the shade, inside a completely dark room, and while using the flash feature of a cellular phone camera, as shown in Figure S10b. The $\lambda_{dominant}$ values were almost constant at 496 nm under all conditions, indicating that the effect exerted by light on the final results of the $\lambda_{dominant}$ was negligible. As such, very little light was required to focus the cellular phone's camera for sensing purposes. Thus, the normal conditions for cellular phone imaging were under ordinary light (i.e., inside the laboratory) with a sample-to-camera distance of ~15 cm.

Human Sweat Test. The measurable metal ions present in human sweat with the photonic IPN_{urease} are Na^+ and K^+.[51,52] Therefore, the responsiveness of the photonic IPN_{urease} film was tested against these metal ions. Figure S10c shows the λ_{PBG} and $\lambda_{dominant}$ values of the photonic IPN_{urease} films 1 h after the dropwise addition of DI pure without salts, as well as NaCl (100 mM) and KCl (100 mM) aqueous solutions (15 μL). The concentrations of the metal ions were controlled at higher than normal concentrations in human sweat; generally, the concentrations of Na^+ and K^+ in human sweat are 50 and 10 mM, respectively.[51] In our case, the λ_{PBG} and $\lambda_{dominant}$ values obtained were 506 ± 7 and 510 ± 8 nm, respectively, for all three samples (including the pure DI water), indicating that Na^+ and K^+ ions did not affect the urea-detecting performance of the photonic IPN_{urease} films. Artificial sweat samples were prepared without urea (C_{urea} = 0 mM) and with urea (C_{urea} = 50 mM) to determine the effect of the other components of human sweat on the color change noted in the IPN_{urease} photonic films on the PDMS chip. Figure 6a shows the photographs (insets) of the PDMS chip 1 h after injecting the artificial sweat samples at C_{urea} = 0 and 50 mM. The flow rate of the syringe pump was maintained at 35 μL/min to mimic the typical sweating rate observed on the human epidermis. The reflected color of the IPN_{urease} photonic film remained green at C_{urea} = 0 mM but became red when C_{urea} was 50 mM. This indicated that the components of human sweat without urea did not affect the reflected color, whereas the components of human sweat with high amounts of urea altered the reflected color observed. Therefore, the PDMS chip developed in this study could be used to enable the selective detection of urea in human sweat.

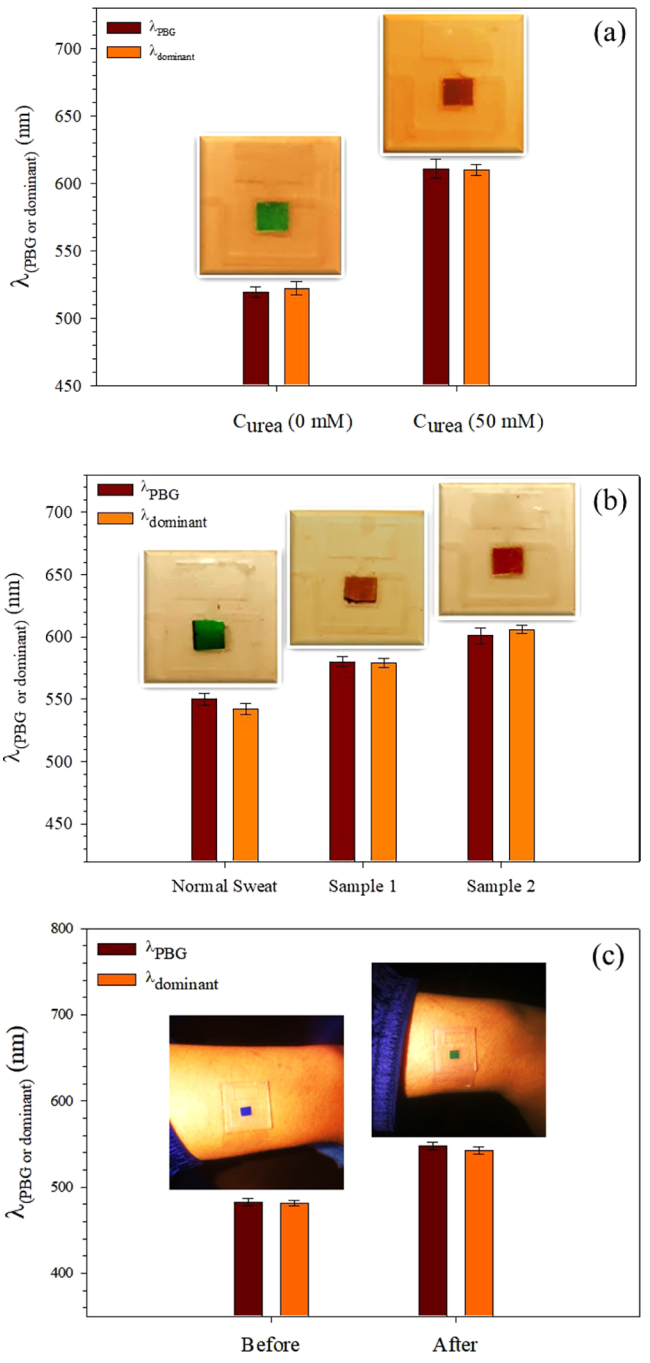

Figure 6. $\lambda_{dominant}$ and λ_{PBG} values of the (a, b) PDMS chip after injecting (a) artificial sweat samples at C_{urea} = 0 and 50 mM and (b) real human sweat samples at C_{urea} = 20 (human sweat), 35 (sample 1), and 45 (sample 2) mM. Sample 1 and sample 2 were prepared by mixing extra urea with human sweat. (c) $\lambda_{dominant}$ and λ_{PBG} values of the PDMS chip attached to the forearm of a healthy volunteer before (without sweat) and after completing a running exercise (with sweat). The brown and orange bars in (a), (b) and (c) represent λ_{PBG} and $\lambda_{dominant}$, respectively. The error bars show the standard deviation for the experiments conducted in triplicate. The insets in (a–c) are real photographs of the respective PDMS chips.

https://dx.doi.org/10.1021/acssensors.0c01757
ACS Sens. XXXX, XXX, XXX−XXX

The developed PDMS chip was then used to test real sweat samples. Here, two uremia samples were prepared by mixing excess urea with human sweat. The total C_{urea} values of human sweat, sample 1, and sample 2 were 20, 35, and 45 mM, respectively. Figure 6b illustrates the $\lambda_{dominant}$ and λ_{PBG} values of the PDMS-embedded photonic IPN_{urease} films tested using donated human sweat, sample 1, and sample 2 (the accompanying photographs are in the inset). Here, the $\lambda_{dominant}$ (and λ_{PBG}) values were 541 (550), 581 (582), and 605 (604) nm for the human sweat, sample 1, and sample 2 samples, respectively. The measured C_{urea} values derived from the standard curve (for λ_{PBG} in Figure S7) were 17.5, 32.7, and 43.3 mM for the human sweat, sample 1, and sample 2, respectively. These values were close to the 20, 35, and 45 mM of the total C_{urea} values. From this, we concluded that the developed photonic IPN_{urease} films could be applied as effective biosensors for the detection of urea in human sweat.

On-body sweat analysis of the prepared PDMS chip was demonstrated on a healthy volunteer, who had no previous record of kidney diseases. Figure 6c shows the PDMS chip patched to the forearm of the healthy volunteer before (without sweat) and after completing a running exercise (with sweat). The reflected color of the photonic IPN_{urease} films in the PDMS chip changed from cyan to green within 1 h after starting the exercise. The $\lambda_{dominant}$ (and λ_{PBG}) values obtained were 541 (547) nm, which led to the calculated C_{urea} of 17.5 ± 0.2 (18 ± 0.2) mM from the standard curve (Figure S7) representing human sweat derived from a healthy volunteer. Thus, the soft, nonirritating PDMS chip prepared in our study could be used for the direct collection and analysis of human sweat in situ. This technology has potential use in military applications and can be extended to the athletic field for marathon runners and rock climbers to gain insight into the medical condition of the wearer.

We developed the photonic IPN flexible film in the patchable PDMS chip for sensing urea in human sweat. This photonic IPN film is flexible, nonirritating, easy patching to the human epidermis, cost-effective, and battery-free. The urea content in sweat can be quantitatively analyzed by the *xy* coordinates of the chromaticity diagram with a simple cellular phone camera without the help of sophisticated analytical instruments. However, the photonic IPN film has some limitations such as long retention time (60 min), shooting angle requirement (~90° against human skin) during taking images of the IPN film, and minimum light. This sensor was optimized in the normal pH range (5.4−6.5) of sweat, while the non-physiological pH (>7) of sweat can affect the result of the sensor.

CONCLUSIONS

A flexible photonic IPN_{urease} film on a PET substrate could be successfully applied as a patchable PDMS chip on the human epidermis for the in situ monitoring of the urea content in human sweat. The PDMS chip, which was designed to collect and transfer sweat to the photonic IPN_{urease} film while allowing excess sweat to drain away, can be used to detect abnormally high urea concentrations in sweat. The naked-eye visualization of the quantitative results was facilitated via changes in the reflected color of the film. This visual quantification was achieved via the calculated $\lambda_{dominant}$ obtained through cellular phone images and a downloadable image app. The developed PDMS biosensor chip provides a simple, convenient, and cost-effective method for urea detection without the need for sophisticated analytical instruments. Through the incorporation of other biosensors, this technology can be expanded for the detection of other analytes. The platform technology using a downloadable cellular phone app facilitates analysis in the remote field or at home where the lab facilities are not available. We believe that this PDMS chip is close to commercialization due to its easy fabrication with commercially available materials.

ASSOCIATED CONTENT

Supporting Information

The Supporting Information is available free of charge at https://pubs.acs.org/doi/10.1021/acssensors.0c01757.

CAD design and photographic image of the aluminum mold, PDMS chip, standard calibration curve from the HPLC spectrum, SEM images of the CLC_{solid} and photonic IPN films, FTIR spectra, $\lambda_{dominant}$ values as a function of λ_{PBG}, CIE 1931 *xy* chromaticity diagrams, photographs and UV−vis spectra at different retention times ($t_{retention}$), λ_{PBG} and $\lambda_{dominant}$ as a function of C_{urea}, $\lambda_{dominant}$ and λ_{PBG} values, and movie during injection of the aqueous urea solution (40 mM) into the PDMS chip (PDF)

AUTHOR INFORMATION

Corresponding Author

Soo-young Park − *School of Applied Chemical Engineering, Polymeric Nano Materials Laboratory, Kyungpook National University, Daegu 41566, Republic of Korea;* orcid.org/0000-0001-6796-4929; Email: psy@knu.ac.kr

Author

Saddam Hussain − *School of Applied Chemical Engineering, Polymeric Nano Materials Laboratory, Kyungpook National University, Daegu 41566, Republic of Korea*

Complete contact information is available at: https://pubs.acs.org/10.1021/acssensors.0c01757

Notes

The authors declare no competing financial interest.

ACKNOWLEDGMENTS

This work was supported by the National Research Foundation of Korea (2020R1A2B5B02001556).

REFERENCES

(1) Lim, H. R.; Kim, H. S.; Qazi, R.; Kwon, Y. T.; Jeong, J. W.; Yeo, W. H. Advanced Soft Materials, Sensor Integrations, and Applications of Wearable Flexible Hybrid Electronics in Healthcare, Energy, and Environment. *Adv. Mater.* **2020**, *32*, No. 1901924.

(2) Gu, Y.; Zhang, T.; Chen, H.; Wang, F.; Pu, Y.; Gao, C.; Li, S. Mini review on flexible and wearable electronics for monitoring human health information. *Nanoscale Res. Lett.* **2019**, *14*, 1−15.

(3) Liu, Y.; Wang, H.; Zhao, W.; Zhang, M.; Qin, H.; Xie, Y. Flexible, stretchable sensors for wearable health monitoring: sensing mechanisms, materials, fabrication strategies and features. *Sensors* **2018**, *18*, 645.

(4) Qiao, Y.; Wang, Y.; Tian, H.; Li, M.; Jian, J.; Wei, Y.; Tian, Y.; Wang, D.-Y.; Pang, Y.; Geng, X.; et al. Multilayer graphene epidermal electronic skin. *ACS Nano* **2018**, *12*, 8839−8846.

(5) Liu, Y.; Pharr, M.; Salvatore, G. A. Lab-on-skin: a review of flexible and stretchable electronics for wearable health monitoring. *ACS Nano* **2017**, *11*, 9614−9635.

(6) Jadoon, S.; Karim, S.; Akram, M. R.; Kalsoom Khan, A.; Zia, M. A.; Siddiqi, A. R.; Murtaza, G. Recent developments in sweat analysis and its applications. *Int. J. Anal. Chem.* **2015**, *2015*, 1−7.

(7) Liang, X.; Boppart, S. A. Biomechanical properties of in vivo human skin from dynamic optical coherence elastography. *IEEE Trans. Biomed. Eng.* **2010**, *57*, 953−959.
(8) Chung, M.; Fortunato, G.; Radacsi, N. Wearable flexible sweat sensors for healthcare monitoring: a review. *J. R. Soc., Interface* **2019**, *16*, No. 20190217.
(9) Guinovart, T.; Bandodkar, A. J.; Windmiller, J. R.; Andrade, F. J.; Wang, J. A potentiometric tattoo sensor for monitoring ammonium in sweat. *Analyst* **2013**, *138*, 7031−7038.
(10) Jia, J.; Xu, C.; Pan, S.; Xia, S.; Wei, P.; Noh, H. Y.; Zhang, P.; Jiang, X. Conductive thread-based textile sensor for continuous perspiration level monitoring. *Sensors* **2018**, *18*, No. 3775.
(11) Wang, T.; Ramnarayanan, A.; Cheng, H. Real time analysis of bioanalytes in healthcare, food, zoology and botany. *Sensors* **2018**, *18*, No. 5.
(12) Bandodkar, A. J.; Gutruf, P.; Choi, J.; Lee, K.; Sekine, Y.; Reeder, J. T.; Jeang, W. J.; Aranyosi, A. J.; Lee, S. P.; Model, J. B.; et al. Battery-free, skin-interfaced microfluidic/electronic systems for simultaneous electrochemical, colorimetric, and volumetric analysis of sweat. *Sci. Adv.* **2019**, *5*, No. eaav3294.
(13) Koh, A.; Kang, D.; Xue, Y.; Lee, S.; Pielak, R. M.; Kim, J.; Hwang, T.; Min, S.; Banks, A.; Bastien, P.; Rogers, J. A.; et al. A soft, wearable microfluidic device for the capture, storage, and colorimetric sensing of sweat. *Sci. Transl. Med.* **2016**, *8*, 366ra165.
(14) Shrivastava, S.; Trung, T. Q.; Lee, N.-E. Recent progress, challenges, and prospects of fully integrated mobile and wearable point-of-care testing systems for self-testing. *Chem. Soc. Rev.* **2020**, *49*, 1812−1866.
(15) Nyein, H. Y. Y.; Bariya, M.; Kivimäki, L.; Uusitalo, S.; Liaw, T. S.; Jansson, E.; Ahn, C. H.; Hangasky, J. A.; Zhao, J.; Lin, Y.; et al. Regional and correlative sweat analysis using high-throughput microfluidic sensing patches toward decoding sweat. *Sci. Adv.* **2019**, *5*, No. eaaw9906.
(16) Kim, S. B.; Koo, J.; Yoon, J.; Hourlier-Fargette, A.; Lee, B.; Chen, S.; Jo, S.; Choi, J.; Oh, Y. S.; Lee, G.; et al. Soft, skin-interfaced microfluidic systems with integrated enzymatic assays for measuring the concentration of ammonia and ethanol in sweat. *Lab Chip* **2020**, *20*, 84−92.
(17) Yang, Y.; Gao, W. Wearable and flexible electronics for continuous molecular monitoring. *Chem. Soc. Rev.* **2019**, *48*, 1465−1491.
(18) Weiner, I. D.; Mitch, W. E.; Sands, J. M. Urea and ammonia metabolism and the control of renal nitrogen excretion. *Clin. J. Am. Soc. Nephrol.* **2015**, *10*, 1444−1458.
(19) Huang, C.-T.; Chen, M.-L.; Huang, L.-L.; Mao, I.-F. Uric acid and urea in human sweat. *Chin. J. Physiol.* **2002**, *45*, 109−115.
(20) Gowda, S.; Desai, P. B.; Kulkarni, S. S.; Hull, V. V.; Math, A. A.; Vernekar, S. N. Markers of renal function tests. *North Am. j. Med. Sci.* **2010**, *2*, 170−173.
(21) Gao, W.; Emaminejad, S.; Nyein, H. Y. Y.; Challa, S.; Chen, K.; Peck, A.; Fahad, H. M.; Ota, H.; Shiraki, H.; Kiriya, D.; et al. Fully integrated wearable sensor arrays for multiplexed in situ perspiration analysis. *Nature* **2016**, 509−514.
(22) Yang, Y.; Song, Y.; Bo, X.; Min, J.; Pak, O. S.; Zhu, L.; Wang, M.; Tu, J.; Kogan, A.; Zhang, H.; Hsiai, T. K.; Li, Z.; Gao, W. A laser-engraved wearable sensor for sensitive detection of uric acid and tyrosine in sweat. *Nat. Biotechnol.* **2020**, *38*, 217−224.
(23) Liu, C.; Xu, T.; Wang, D.; Zhang, X. J. T. The role of sampling in wearable sweat sensors. *Talanta* **2020**, *212*, No. 120801.
(24) Liu, Y.-L.; Liu, R.; Qin, Y.; Qiu, Q.-F.; Chen, Z.; Cheng, S.-B.; Huang, W.-H. Flexible electrochemical urea sensor based on surface molecularly imprinted nanotubes for detection of human sweat. *Anal. Chem.* **2018**, *90*, 13081−13087.
(25) Soni, A.; Surana, R. K.; Jha, S. K. Smartphone based optical biosensor for the detection of urea in saliva. *Sens. Actuators, B* **2018**, *269*, 346−353.
(26) Ligler, F. S.; Taitt, C. R. *Optical Biosensors: Present & Future*; Gulf Professional Publishing, 2002.
(27) Grieshaber, D.; MacKenzie, R.; Vörös, J.; Reimhult, E. Electrochemical biosensors-sensor principles and architectures. *Sensors* **2008**, *8*, 1400−1458.
(28) Noh, K. G.; Park, S. Y. Biosensor Array of Interpenetrating Polymer Network with Photonic Film Templated from Reactive Cholesteric Liquid Crystal and Enzyme-Immobilized Hydrogel Polymer. *Adv. Funct. Mater.* **2018**, *28*, No. 1707562.
(29) Vallejos, S.; Hernando, E.; Trigo, M.; García, F. C.; García-Valverde, M.; Iturbe, D.; Cabero, M. J.; Quesada, R.; García, J. M. Polymeric chemosensor for the detection and quantification of chloride in human sweat. Application to the diagnosis of cystic fibrosis. *J. Mater. Chem. B* **2018**, *6*, 3735−3741.
(30) Yetisen, A. K.; Moreddu, R.; Seifi, S.; Jiang, N.; Vega, K.; Dong, X.; Dong, J.; Butt, H.; Jakobi, M.; Elsner, M.; Koch, A. W. Dermal Tattoo Biosensors for Colorimetric Metabolite Detection. *Angew. Chem.* **2019**, *131*, 10616−10623.
(31) Moreddu, R.; Wolffsohn, J. S.; Vigolo, D.; Yetisen, A. K. Laser-inscribed contact lens sensors for the detection of analytes in the tear fluid. *Sens. Actuators, B* **2020**, *317*, No. 128183.
(32) Kim, J.-S.; Oh, H.-B.; Kim, A.-H.; Kim, J.-S.; Lee, E.-S.; Baek, J.-Y.; Lee, K. S.; Chung, S.-C.; Jun, J.-H. A study on detection of glucose concentration using changes in color coordinates. *Bioengineered* **2017**, *8*, 99−104.
(33) Zhang, Y.; Guo, H.; Kim, S. B.; Wu, Y.; Ostojich, D.; Park, S. H.; Wang, X.; Weng, Z.; Li, R.; Bandodkar, A. J.; et al. Passive sweat collection and colorimetric analysis of biomarkers relevant to kidney disorders using a soft microfluidic system. *Lab Chip* **2019**, *19*, 1545−1555.
(34) He, X.; Xu, T.; Gu, Z.; Gao, W.; Xu, L.-P.; Pan, T.; Zhang, X. Flexible and superwettable bands as a platform toward sweat sampling and sensing. *Anal. Chem.* **2019**, *91*, 4296−4300.
(35) He, X.; Pei, Q.; Xu, T.; Zhang, X. Smartphone-based tape sensors for multiplexed rapid urinalysis. *Sens. Actuators, B* **2020**, *304*, No. 127415.
(36) Myung, D.-b.; Hussain, S.; Park, S.-Y. Photonic calcium and humidity array sensor prepared with reactive cholesteric liquid crystal mesogens. *Sens. Actuators, B* **2019**, *298*, No. 126894.
(37) Korevaar, P. A.; Kaplan, C. N.; Grinthal, A.; Rust, R. M.; Aizenberg, J. Non-equilibrium signal integration in hydrogels. *Nat. Commun.* **2020**, *11*, 1−10.
(38) Panther, D. J.; Jacob, S. E. The importance of acidification in atopic eczema: an underexplored avenue for treatment. *J. Clin. Med.* **2015**, *4*, 970−978.
(39) Mandrioli, M.; Tura, M.; Scotti, S.; Toschi, T. G. Fast Detection of 10 Cannabinoids by RP-HPLC-UV Method in Cannabis sativa L. *Molecules* **2019**, *24*, No. 2113.
(40) Yarur, F.; Macairan, J.-R.; Naccache, R. Ratiometric detection of heavy metal ions using fluorescent carbon dots. *Environ. Sci.: Nano* **2019**, *6*, 1121−1130.
(41) Wenzl, T.; Haedrich, J.; Schaechtele, A.; Piotr, R.; Stroka, J.; Eppe, G.; Scholl, G. *Guidance Document on the Estimation of LOD and LOQ for Measurements in the Field of Contaminants in Food and Feed*; Institute for Reference Materials and Measurements (IRMM), 2016.
(42) Best, J. *Colour Design: Theories and Applications*; Woodhead Publishing, 2017.
(43) Kang, H. R. *Color Technology for Electronic Imaging Devices*; SPIE press, 1997.
(44) Myung, D.-b.; Hussain, S.; Park, S.-Y. Photonic calcium and humidity array sensor prepared with reactive cholesteric liquid crystal mesogens. *Sens. Actuators, B* **2019**, *298*, No. 126894.
(45) Dong, J.; Ozaki, Y.; Nakashima, K. FTIR studies of conformational energies of poly (acrylic acid) in cast films. *J. Polym. Sci., Part B: Polym. Phys.* **1997**, *35*, 507−515.
(46) Di Foggia, M.; Taddei, P.; Torreggiani, A.; Dettin, M.; Tinti, A. Self-assembling Peptides for Biomedical Applications: IR and Raman Spectroscopies for the Study of Secondary Structure. *Proteomics Res. J.* **2011**, *2*, 231−272.
(47) Zhang, Y.; Guo, H.; Kim, S. B.; Wu, Y.; Ostojich, D.; Park, S. H.; Wang, X.; Weng, Z.; Li, R.; Bandodkar, A. J.; et al. Passive sweat

https://dx.doi.org/10.1021/acssensors.0c01757
ACS Sens. XXXX, XXX, XXX−XXX

collection and colorimetric analysis of biomarkers relevant to kidney disorders using a soft microfluidic system. *Lab Chip* **2019**, *19*, 1545−1555.
(48) Chen, M.-M.; Cheng, S.-B.; Ji, K.; Gao, J.; Liu, Y.-L.; Wen, W.; Zhang, X.; Wang, S.; Huang, W.-H. Construction of a flexible electrochemiluminescence platform for sweat detection. *Chem. Sci.* **2019**, *10*, 6295−6303.
(49) Liu, Y.-L.; Liu, R.; Qin, Y.; Qiu, Q.-F.; Chen, Z.; Cheng, S.-B.; Huang, W.-H. Flexible electrochemical urea sensor based on surface molecularly imprinted nanotubes for detection of human sweat. *Anal. Chem.* **2018**, *90*, 13081−13087.
(50) Choi, J.; Kang, D.; Han, S.; Kim, S. B.; Rogers, J. A. Thin, Soft, Skin-Mounted Microfluidic Networks with Capillary Bursting Valves for Chrono-Sampling of Sweat. *Adv. Healthcare Mater.* **2017**, *6*, No. 1601355.
(51) Holmes, N.; Bates, G.; Zhao, Y.; Sherriff, J.; Miller, V. The effect of exercise intensity on sweat rate and sweat sodium and potassium losses in trained endurance athletes. *Ann. Sports Med. Res.* **2016**, *3*, 1−4.
(52) Stekolshchikova, A. A.; Radaev, A. V.; Orlova, O. Y.; Nikolaev, K. G.; Skorb, E. V. Thin and Flexible Ion Sensors Based on Polyelectrolyte Multilayers Assembled onto the Carbon Adhesive Tape. *ACS Omega* **2019**, *4*, 15421−15427.

https://dx.doi.org/10.1021/acssensors.0c01757
ACS Sens. XXXX, XXX, XXX−XXX